Available online at www.sciencedirect.com
SCIENCE DIRECT®
International Journal of Heat and Mass Transfer 49 (2006) 171–186
International Journal of HEAT and MASS TRANSFER
www.elsevier.com/locate/ijhmt

Choking flow modeling with mechanical and thermal non-equilibrium

H.J. Yoon *, M. Ishii, S.T. Revankar

School of Nuclear Engineering, Purdue University, West Lafayette, IN 47907, United States

Received 24 May 2005; received in revised form 20 July 2005
Available online 1 December 2005

Abstract

The mechanistic model, which considers the mechanical and thermal non-equilibrium, is described for two-phase choking flow. The choking mass flux is obtained from the momentum equation with the definition of choking. The key parameter for the mechanical non-equilibrium is a slip ratio. The dependent parameters for the slip ratio are identified. In this research, the slip ratio which is defined in the drift flux model is used to identify the impact parameters on the slip ratio. Because the slip ratio in the drift flux model is related to the distribution parameter and drift velocity, the adequate correlations depending on the flow regime are introduced in this study. For the thermal non-equilibrium, the model is developed with bubble conduction time and Bernoulli choking model. In case of highly subcooled water compared to the inlet pressure, the Bernoulli choking model using the pressure undershoot is used because there is no bubble generation in the test section. When the phase change happens inside the test section, two-phase choking model with relaxation time calculates the choking mass flux. According to the comparison of model prediction with experimental data shows good agreement. The developed model shows good prediction in both low and high pressure ranges.

Keywords: Choking mass flux; Mechanical non-equilibrium; Thermal non-equilibrium; Slip ratio; Relaxation

1. Introduction

The choking flow is the phenomenon which occurs in very wide range of engineering industry. This phenomenon is the most important in the nuclear power plant which is cooled by the water. In the loss of coolant accident (LOCA) situation, the choking flow determined the water inventory of the reactor vessel, and the integrity of core eventually depends upon the choking flow [1]. Therefore, the analytical description and prediction of choking flow rate plays an important role in the design of the engineered safeguards in the nuclear power plant. The serious study for two-phase flow started from 1892 by Sauvage [2]. Rateau [3] showed the existence of choking flow in the boiling water through the nozzle. Historically mechanical and thermal equilibrium between gas and liquid phases were commonly assumed in the early choking flow models. This model is called the homogeneous equilibrium model. However, this assumption is valid only for some ideal conditions such as for a long pipe where there is sufficient time for equilibrium to be achieved and when the flow pattern gives sufficient interphase forces to suppress significant relative motion.

* Corresponding author. Tel.: +1 765 494 4678; fax: +1 765 494 9570.
E-mail address: hyoon@purdue.edu (H.J. Yoon).

0017-9310/$ - see front matter © 2005 Published by Elsevier Ltd.
doi:10.1016/j.ijheatmasstransfer.2005.07.044

Nomenclature

A	area
C_o	distribution parameter
c_p	specific heat
D	diameter
D_d	bubble departure diameter
f_d	bubble departure frequency
F	function
g	gravitational acceleration
G	mass flux (kg/m^2 s)
h	enthalpy
J	multiplier
k	Boltzmann constant
L	length
$\dot{m}$	mass flow rate
P	pressure
s	entropy
S	slip ratio
t	time
T	temperature
T_c	critical temperature
T_r	reduced temperature
V	velocity
$\langle\langle V_{gj}\rangle\rangle$	weighted drift velocity
$\overline{V}_{gj}$	mean drift velocity
x	quality
z	axial distance

Greek symbols

α	void fraction
β	volumetric thermal expansion coefficient
Γ	mass change rate
θ	contact angle
ρ	density
Σ	depressurization rate
τ	shear stress, relaxation time

Subscripts

c	choking
char	characteristic
cond	conduction
down	downstream
e	equilibrium
f	liquid
fl	flashing
g	vapor or gas phase
growth	bubble growth
i	interface
in	inlet or initial
m	mixture
nucl	nucleation
o	stagnation
s	saturation
sat	saturation
sub	subcooling
tot	total
up	upstream
w	wall
x–s	cross-section

2. Review of choking flow models

It is also important to understand the existing choking flow models. In this section, the choking flow models are classified as homogeneous equilibrium, homogeneous non-equilibrium, non-homogeneous equilibrium, and non-homogeneous non-equilibrium model.

2.1. Homogeneous equilibrium model

According to Starkmann's homogeneous equilibrium model [4], it is based on the assumptions of no slip, thermal equilibrium between phases, isentropic expansion and equation of state in the steam table. According to this model the choking mass flux in the homogeneous equilibrium model depends not on the break geometry or pipe length but on the upstream thermodynamic condition.

A feature of the homogeneous equilibrium model is adherence of the fluid properties along the saturation condition. In reality, the liquid can be superheated in order to nucleate near the wall during the depressurization process. If the single-phase liquid velocity is high enough, the choking flow may occur at the outlet of the pipe with the nucleation of the first bubble. If the coolant temperature is low and nucleation is suppressed by non-equilibrium phenomena, it might be required to consider the transition from single-phase to two-phase choking flow during the early stage of a blowdown in a LOCA analysis [5]. According to the review of Abdollahian et al. [6], the homogeneous equilibrium model showed good agreement with the Marviken critical flow data for subcooled stagnation condition and long pipe condition ($L/D > 1.5$). However, in general, the homogeneous equilibrium model is the simplest approach and not highly accurate for the subcooled liquid stagnation state [1]. Recently, Fthenakis et al. [7] showed that the homogeneous equilibrium model can overestimate the choking flow rate in case that the break is large, and that makes the rapid depressurization. However,

according to results of Darby [8], the homogeneous equilibrium model underestimated the choking flow rate in short pipe. In that reference, the homogeneous equilibrium model is applicable for the long pipe because this model is based on the no slip velocity, whereas, there is no sufficient time to establish the mechanical equilibrium in the short pipe. However, the homogeneous equilibrium model overestimates the mixture density in case of large break, and this results in more liquid being discharged through the break. Therefore, the homogeneous equilibrium model overestimates the choking flow rate at the break.

As a different approach of the homogeneous equilibrium model, there is Omega method. The analytical solution using this method was first proposed by Epstein et al. [9] for the steam-water mixture, and generalized by Leung [10] for any flashing two-phase mixture. They introduced the approximate equation of state. The author pointed out that the homogeneous equilibrium model was physically unrealistic. However, the opinion of author was that this model was valuable for understanding qualitative features of two-phase choking, using in scaling law, and estimating quantitative prediction [11].

2.2. Homogeneous non-equilibrium model

Thermal non-equilibrium implies that there is a temperature difference between the phases. This is believed to be one of the major causes of the discrepancy between model predictions and experimental results, especially if subcooled fluid enters the test section or the test section is very short. According to the review presented by Abdollahian et al. [6] and Saha [12], one particular type of choking flow has escaped full understanding to date, even though a number of theoretical and experimental studies of choking flow have been reported. It occurs with a subcooled upstream condition that often leads to significant non-equilibrium thermodynamic conditions at the point of choking flow. At that point the liquid is superheated beyond the saturation temperature. This non-equilibrium effect is generated because the two-phase fluid depressurization speed may be faster than the thermal exchange speed between two phases [13].

Actually, thermal non-equilibrium is related to the bubble nucleation. This was proven by several researchers using a delay time for nucleation time of order of 1 ms [14,15]. Fauske [16] showed a good agreement using the "relaxation length" by comparing with other data. This "relaxation time" or "relaxation length" corresponds to the super heat of 2–3 °C.

Henry and Fauske [17] tried to account for the thermal non-equilibrium effect by introducing an empirical parameter, which represented the deviation from the homogeneous equilibrium model. This model assumed the phase separation at the entrance and neglected the friction loss. It is directly proportional to the difference between the exit qualities. However, Abdollahian et al. [6] pointed out that the Henry–Fauske model in the subcooled flow regime overpredicted the Marviken data.

Shrock et al. [15] developed a two-step model. Initially "frozen" flow (constant quality) is assumed until the pressure drops by a certain amount below the saturation pressure. At that point sudden equilibrium is achieved, and downstream from this point, again the frozen flow occurs. It was stated by the authors that the model did not represent the real physical behavior, however, they claimed that there was no satisfactory means to predict the number and size of microbubble in the liquid triggering the nucleation process.

Levy and Abdollahian [18] developed the simplified homogeneous non-equilibrium flashing model. This model assumed that water should be superheated at a given local pressure before liquid flashed into steam and that in downstream enough vapor would be generated to reduce the water superheat. In addition, the flow was assumed to be homogeneous. Finally, an isentropic process was used to calculate the non-equilibrium quality and choking flow rate. This model was compared with the data of Reocreux [19] and Zimmer et al. [20]. For those two data sets, this model's prediction was reasonable. However, the model may not properly account for the impact of depressurization rate upon non-equilibrium conditions. In addition, it underpredicts small scale tests at high pressures when a constant cross-section length does not follow the contraction zone.

Finally, there is the frozen model as it is referred previously. This model is the limiting case of the homogeneous non-equilibrium model and it is based on the assumption of no heat and mass transfer between phases. Lenzing et al. [21] used the homogeneous frozen flow model by introducing the two-phase discharge coefficient for the non-flashing two-component flow and Henry and Fauske model by using the two-phase discharge coefficient for the flashing one-component flow.

2.3. Non-homogeneous equilibrium model

The early model of the non-homogeneous equilibrium model derived by Moody [22] is an extension of the homogeneous equilibrium model, by allowing different vapor and liquid velocities. A slip ratio, S, defined as the velocity ratio between the vapor and liquid, is treated as a variable which is determined by the condition of maximum kinetic energy flux at the exit. The slip between two phases allows the gas phase to be discharged with the higher velocity than liquid phase and this is more realistic approach than the homogeneous flow assumption [7]. Moody model gives the local slip ratio of $S = V_g/V_f = (\rho_f/\rho_g)^{1/3}$ to get a maximum two-phase kinetic energy flow, whereas Fauske [23] obtains the slip ratio as $S = V_g/V_f = (\rho_f/\rho_g)^{1/2}$ by minimizing

the momentum flow rate. The detailed description was shown in ANL report based on the author's thesis [24]. Fauske emphasized the importance of the mechanical non-equilibrium in terms of the slip. According to Fauske's thesis, the slip is generated due to the density ratio between two phases and, therefore, light phase is easily accelerated by means of pressure difference between the upstream and choking section. The author also insisted that the friction between the phases and droplet caused by the liquid entrainment reduces the relative velocity between two phases. However, Fauske insisted that the slip is independent of the quality using other results [25]. According to their experimental results, the effect of slip ratio decreased with pressure increase. According to Fauske, the superficial velocity in choking condition is much high, therefore, it is reasonable that the slip ratio does not affected by the quality.

However, the weak point of these models is that they are derived based on the ideal flow patterns, annular or separated flow. Furthermore, they are based on the energy or momentum maximization or minimization assumption which has no theoretical bases and the slip ratio is not independent of the quality. Cruver and Moulton [26] pointed out the problem in the assumptions of Fauske's theorem. In the Fauske's thesis, the author assumed that the pressure gradient at the choking point is a finite maximum. However, according to Cruver and Moulton's opinion, $\partial v_m/\partial S$ is a minimum, not a maximum because $\partial^2 v_m/\partial S^2 = 2x(1-x)v_g/S^3$ is always positive. Therefore, they insist that the finite maximum for dP/dz does not exist.

2.4. Non-homogeneous non-equilibrium model

In the two-fluid model, it is possible to consider the mechanical non-equilibrium and the thermal non-equilibrium simultaneously through proper constitutive relations for interfacial transfer rates.

In this approach, a separate set of conservation equations is used for each phase as shown by Bouré [27] and Ishii [28]. Therefore, these equations have to contain terms describing mass, momentum and heat transfer between the phases. These constitutive relations are not very accurate in the present state-of the art, particularly under the choking flow conditions where very large convective acceleration and depressurization take place. Thus simplification of the above equations and often quite arbitrary assumptions are introduced to overcome the lack of knowledge. The separate flow model is easy to visualize the mechanical non-equilibrium and thermal non-equilibrium between phases, however, the actual geometry of the interface can be quite different from this flow due to wall nucleation and flashing.

The typical existing interfacial exchange models were described by Trapp and Ransom [29]. Possible weakness of their model involves the modeling of non-equilibrium mass and heat transfer terms, thermal resistance to heat flux, virtual mass coefficient, and the use of derivatives of the equations of state in thermal equilibrium. This implies that the interfacial momentum and energy in highly non-equilibrium flow may not be accurately modeled by the conventional models in the code, particularly due to the significant nucleation at the wall which is difficult to predict.

Richter [30] developed the separated flow model to calculate the choking flow rate for the steam-water mixture. Generally, the separate flow model requires several correlations for the unknown parameters. However, it deals both mechanical and thermal non-equilibrium in one approach. This model was considered with the assumptions of steady state, one dimensional, and non-homogeneous flow. Additionally, it was assumed that heat transfer between phases limited mass transfer.

According to Richter's results, the slip ratio in the bubbly flow regime was about unity and it was reasonable to assume this as many authors assumed. However, the author insisted that if the evaporation in expanding bubbly flow was limited by heat transfer, the small velocity difference played an important role in the heat transfer mechanism. For the churn-turbulent flow regime, the author concluded that the thermal non-equilibrium was negligible and the mechanical no-equilibrium was dominant in this flow regime. Although the result was very interesting, his results depended on the chosen correlation when this model was solved, and it was questionable whether it might be applicable to the low pressure.

3. Modeling description

The main objective of this research is to develop the mechanistic choking model which considers the mechanical and thermal non-equilibrium. In the view of the liquid and gas velocity, it is homogeneous flow if both velocities are same. As the non-homogeneous flow, there are two types of non-homogeneous flow, mechanical equilibrium flow and mechanical non-equilibrium flow. Even though both velocities are different, if the relative velocity ($V_g - V_f$) is steady state, it is the mechanical equilibrium flow. Mechanical non-equilibrium flow is important in the inertia dominant flow. In the nozzle geometry, the pressure drop is mainly caused by the acceleration of each phase. In addition, near the choking point, acceleration rates of each phase, DV_f/Dt and DV_g/Dt, are different. Therefore, the modeling for mechanical non-equilibrium in the choking flow is very important. In the view of the temperature of each phase, it is called thermal equilibrium if the temperatures of each phase are same. In the rapid depressurization condition which causes flashing, thermal non-equilibrium is present. For example, rapid depressurization of a liquid

system may drop the pressure well below the saturation value corresponding to the temperature of the liquid. In this situation, the liquid tends to remain at the initial temperature, whereas the vapor follows the saturation temperature. Consequently there is departure from the thermal equilibrium. Similarly, a subcooled discharge through a break or an orifice may expose fluid particles to a rapid change in pressure. If the downstream pressure is below the saturation value corresponding to the temperature of the liquid, then the fluid flashes in a process similar to that of a rapid depressurization, and there may be similar departure from the thermal equilibrium. As illustrated in Fig. 1, there are two kinds of time delay in the thermal non-equilibrium process. The phase change can only take place in finite speed time. Namely, it takes time for bubble to nucleate and grow. The superheat is required to nucleate the bubble. The pressure undershoot supplies the superheat for bubble generation. Relaxation time for nucleation, τ_{nucl}, indicates the required time to reach the satisfactory pressure undershoot. In the nozzle where there is the rapid pressure drop, relaxation time for nucleation is negligible. More dominant relaxation time is for the bubble growth. As indicated in Fig. 1, the thermal equilibrium can be established with τ_{growth}. In this research, it is assumed that the thermal equilibrium is valid when the bubble departs from the wall. The bubble growth from the wall is governed by the conduction between the vapor and super heated liquid. Therefore, τ_{growth} means the conduction time to bubble depart.

In writing the momentum equation of the separated flow, several assumptions are made in advance, namely: (i) The surface tension, Reynolds stress, and virtual mass effects are assumed to be small enough to be neglected, and (ii) The pressure of each phase is assumed to be equal. The momentum equations for the liquid and gas phase are as follows:

Liquid phase

$$-\frac{\partial}{\partial z}[P(1-\alpha)A_{x-s}]\Delta z - P_{\text{i}}\frac{\partial[\alpha A_{x-s}]}{\partial z}\Delta z + P_{\text{w}}\frac{\partial A_{x-s}}{\partial z}\Delta z - g\rho_{\text{f}}(1-\alpha)A_{x-s}\Delta z\sin\theta - \tau_{\text{w}}p_{\text{e}}\Delta z + \tau_{\text{i}}p_{\text{i}}\Delta z = \frac{\partial}{\partial t}[\rho_{\text{f}}(1-\alpha)A_{x-s}V_{\text{f}}\Delta z] + \frac{\partial}{\partial z}[\rho_{\text{f}}(1-\alpha)A_{x-s}V_{\text{f}}^2]\Delta z + A_{x-s}\Gamma V_{\text{i}}\Delta z \quad (1)$$

Gas phase

$$-\frac{\partial}{\partial z}[P\alpha A_{x-s}]\Delta z - P_{\text{i}}\frac{\partial[\alpha A_{x-s}]}{\partial z}\Delta z + P_{\text{w}}\frac{\partial A_{x-s}}{\partial z}\Delta z - g\rho_{\text{g}}\alpha A_{x-s}\Delta z\sin\theta + \tau_{\text{i}}p_{\text{i}}\Delta z = \frac{\partial}{\partial t}[\rho_{\text{g}}\alpha A_{x-s}V_{\text{g}}\Delta z] + \frac{\partial}{\partial z}[\rho_{\text{g}}\alpha A_{x-s}V_{\text{g}}^2]\Delta z - A_{x-s}\Gamma V_{\text{i}}\Delta z \quad (2)$$

where τ is the shear stress. The subscripts 'w' and 'i' denote the wall and interface.

For steady state flow, additional assumptions are considered such that (i) The radial pressure gradient is assumed to be zero and (ii) the interfacial pressure, P_{i}, and wall pressure, P_{w}, are equal to the static pressure, P. Accounting for the above assumptions, Eqs. (1) and (2) are reduced respectively to

$$-(1-\alpha)\frac{\partial P}{\partial z} - \frac{\tau_{\text{w}}p_{\text{e}}}{A_{x-s}} + \frac{\tau_{\text{i}}P}{A_{x-s}} = \frac{1}{A_{x-s}}\frac{\partial}{\partial z}[\rho_{\text{f}}(1-\alpha)A_{x-s}V_{\text{f}}^2] \quad (3)$$

$$-\alpha\frac{\partial P}{\partial z} - \frac{\tau_{\text{i}}P}{A_{x-s}} = \frac{1}{A_{x-s}}\frac{\partial}{\partial z}[\rho_{\text{g}}\alpha A_{x-s}V_{\text{g}}^2] \quad (4)$$

Hence, by combining Eqs. (3) and (4), the mixture momentum equation is obtained as follows:

$$-\frac{\partial P}{\partial z} - \frac{\tau_{\text{w}}p_{\text{e}}}{A_{x-s}} = \frac{1}{A_{x-s}}\frac{\partial}{\partial z}[\rho_{\text{f}}(1-\alpha)A_{x-s}V_{\text{f}}^2 + \rho_{\text{g}}\alpha A_{x-s}V_{\text{g}}^2] \quad (5)$$

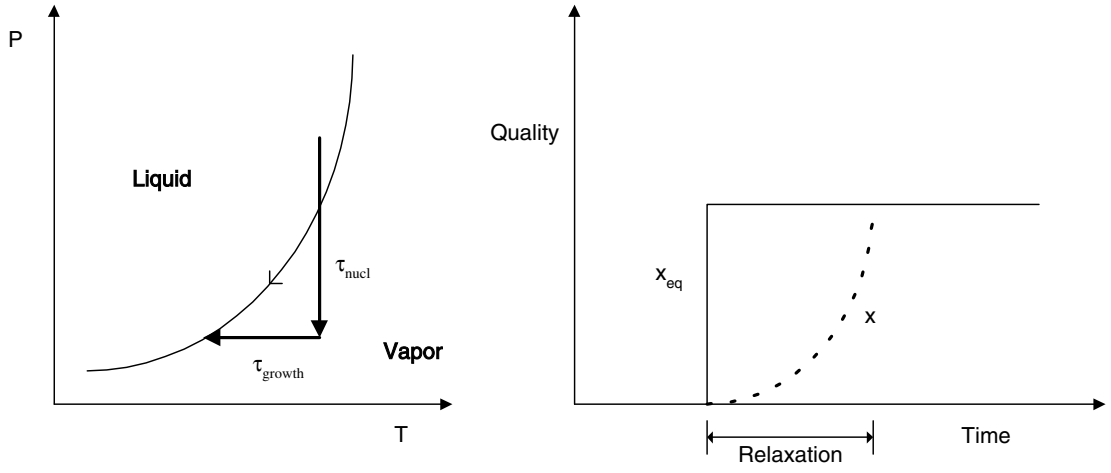

Fig. 1. Thermal non-equilibrium.

In the choking condition, the effect of the wall friction on the pressure drop is negligible compared to that attributed to the convective term. Hence, the pressure drop due to the wall friction is neglected in developing the choking model. Therefore, after rearranging the convective term, the final momentum equation for the choking condition in a separated two-phase flow is given by

$$\begin{aligned}-\frac{\partial P}{\partial z} &= \frac{1}{A_{x-s}}\frac{\partial}{\partial z}[\dot{m}_f V_f + \dot{m}_g V_g] \\ &= G\frac{\partial}{\partial z}[(1-x)V_f + xV_g] \\ &= G\frac{\partial}{\partial z}\{[(1-x)+xS]V_f\} \end{aligned} \tag{6}$$

where $\dot{m}$, G and S denote mass flow rate, mass flux and slip ratio, respectively. The mass flux in Eq. (6) is defined by

$$G = [\alpha\rho_g V_g + (1-\alpha)\rho_f V_f] = [\alpha\rho_g S + (1-\alpha)\rho_f]V_f \tag{7}$$

In the adiabatic condition, the flow quality is not changed even though the void fraction varies due to geometry changes. Therefore, it is more convenient to replace the void fraction with the flow quality. The relationship can be obtained from the continuity equation as

$$\alpha = x\frac{\rho_f}{\rho_g}\Bigg/\left[S(1-x)+x\frac{\rho_f}{\rho_g}\right] \tag{8}$$

The liquid velocity can be expressed by combining Eqs. (7) and (8) as

$$V_f = G\Bigg/\left[\frac{S\rho_f}{S(1-x)+x\frac{\rho_f}{\rho_g}}\right] \tag{9}$$

The modified momentum equation is obtained after inserting Eq. (9) into Eq. (6) as

$$\begin{aligned}-\frac{dP}{dz} &= G\frac{\partial}{\partial z}\left\{(xS+1-x)\cdot\frac{G\left[S(1-x)+x\frac{\rho_f}{\rho_g}\right]}{S\rho_f}\right\} \\ &= \frac{\dot{m}^2}{A_{x-s}}\frac{\partial}{\partial z}\left[\frac{1}{A_{x-s}}(xS+1-x)\cdot\frac{S(1-x)+x\frac{\rho_f}{\rho_g}}{S\rho_f}\right] \end{aligned} \tag{10}$$

The term inside the bracket of the second equation in Eq. (10) is a function of area, flow quality, gas density, liquid density and slip ratio, i.e.,

$$F = F(A_{x-s}, x, \rho_f, \rho_g, S) \tag{11}$$

In general, the flow quality, liquid density and gas density are functions of pressure and entropy. The slip ratio is a function of the quality and pressure. Therefore, differentiation of the term inside bracket with respect to z is expanded by the chain rule as

$$\begin{aligned}\frac{\partial F}{\partial z} &= \frac{\partial F}{\partial S}\frac{\partial S}{\partial z}+\frac{\partial F}{\partial x}\frac{\partial x}{\partial z}+\frac{\partial F}{\partial \rho_f}\frac{\partial \rho_f}{\partial z}+\frac{\partial F}{\partial \rho_g}\frac{\partial \rho_g}{\partial z}+\frac{\partial F}{\partial A_{x-s}}\frac{\partial A_{x-s}}{\partial z} \\ &= \frac{\partial F}{\partial S}\left(\frac{\partial S}{\partial P}\frac{\partial P}{\partial z}+\frac{\partial S}{\partial x}\frac{\partial x}{\partial z}\right)+\frac{\partial F}{\partial x}\left(\frac{\partial x}{\partial P}\frac{\partial P}{\partial z}+\frac{\partial x}{\partial s}\frac{\partial s}{\partial z}\right) \\ &\quad+\frac{\partial F}{\partial \rho_f}\left(\frac{\partial \rho_f}{\partial P}\frac{\partial P}{\partial z}+\frac{\partial \rho_f}{\partial s}\frac{\partial s}{\partial z}\right)+\frac{\partial F}{\partial \rho_g}\left(\frac{\partial \rho_g}{\partial P}\frac{\partial P}{\partial z}+\frac{\partial \rho_g}{\partial s}\frac{\partial s}{\partial z}\right) \\ &\quad+\frac{\partial F}{\partial A_{x-s}}\frac{\partial A_{x-s}}{\partial z} \\ &= \frac{\partial F}{\partial S}\left(\frac{\partial S}{\partial P}\frac{\partial P}{\partial z}+\frac{\partial S}{\partial x}\left(\frac{\partial x}{\partial P}\frac{\partial P}{\partial z}+\frac{\partial x}{\partial s}\frac{\partial s}{\partial z}\right)\right) \\ &\quad+\frac{\partial F}{\partial x}\left(\frac{\partial x}{\partial P}\frac{\partial P}{\partial z}+\frac{\partial x}{\partial s}\frac{\partial s}{\partial z}\right)+\frac{\partial F}{\partial \rho_f}\left(\frac{\partial \rho_f}{\partial P}\frac{\partial P}{\partial z}+\frac{\partial \rho_f}{\partial s}\frac{\partial s}{\partial z}\right) \\ &\quad+\frac{\partial F}{\partial \rho_g}\left(\frac{\partial \rho_g}{\partial P}\frac{\partial P}{\partial z}+\frac{\partial \rho_g}{\partial s}\frac{\partial s}{\partial z}\right)+\frac{\partial F}{\partial A_{x-s}}\frac{\partial A_{x-s}}{\partial z} \end{aligned} \tag{12}$$

In this research, the flow is assumed to be isentropic, which implies that the entropy does not change along the flow direction. Based on this assumption, the Eq. (12) is expressed as

$$\begin{aligned}\frac{\partial F}{\partial z} &= \frac{\partial F}{\partial S}\left(\frac{\partial S}{\partial P}\frac{\partial P}{\partial z}+\frac{\partial S}{\partial x}\frac{\partial x}{\partial z}\right)+\frac{\partial F}{\partial x}\frac{\partial x}{\partial z}+\frac{\partial F}{\partial \rho_f}\left(\frac{\partial \rho_f}{\partial P}\frac{\partial P}{\partial z}\right) \\ &\quad+\frac{\partial F}{\partial \rho_g}\left(\frac{\partial \rho_g}{\partial P}\frac{\partial P}{\partial z}\right)+\frac{\partial F}{\partial A_{x-s}}\frac{\partial A_{x-s}}{\partial z} \end{aligned} \tag{13}$$

Therefore, rewriting Eq. (13) in terms of pressure drop and comparing it with Eq. (10), the momentum equation is transformed into the following equation:

$$\begin{aligned}-\frac{dP}{dz} &= \frac{\dot{m}^2}{A_{x-s}}\left(\frac{\partial F}{\partial S}\frac{\partial S}{\partial P}\frac{\partial P}{\partial z}+\frac{\partial F}{\partial S}\frac{\partial S}{\partial x}\frac{\partial x}{\partial z}+\frac{\partial F}{\partial x}\frac{\partial x}{\partial z}\right. \\ &\quad\left.+\frac{\partial F}{\partial \rho_f}\frac{\partial \rho_f}{\partial P}\frac{\partial P}{\partial z}+\frac{\partial F}{\partial \rho_g}\frac{\partial \rho_g}{\partial P}\frac{\partial P}{\partial z}+\frac{\partial F}{\partial A_{x-s}}\frac{\partial A_{x-s}}{\partial z}\right) \end{aligned} \tag{14}$$

The second and third terms do not seem to affect the choking flow rate because it is not coupled with the pressure drop. However, it actually contributes to the choking flow rate when there is phase change. Terms inside the parenthesis of the right hand side of Eq. (14), $\partial F/\partial S$, $\partial F/\partial x$, $\partial F/\partial \rho_f$, $\partial F/\partial \rho_g$, and $\partial F/\partial A_{x-s}$, can be obtained from Eq. (10) by partial differentiation.

$$\frac{\partial F}{\partial S} = \frac{1}{A_{x-s}S^2\rho_f}\left\{-x^2S^2-S+Sx+\frac{\rho_f}{\rho_g}x(x-1)\right\} = \frac{\Phi_1}{A_{x-s}} \tag{15}$$

$$\begin{aligned}\frac{\partial F}{\partial x} &= \frac{1}{A_{x-s}S\rho_f}\left\{(1-2x)\left(S^2-S+\frac{\rho_f}{\rho_g}\right)-S\left(1-2x\frac{\rho_f}{\rho_g}\right)\right\} \\ &= \frac{\Phi_2}{A_{x-s}} \end{aligned} \tag{16}$$

$$\frac{\partial F}{\partial \rho_f} = -\frac{(xS+1-x)(1-x)}{A_{x-s}\rho_f^2} = \frac{\Phi_3}{A_{x-s}} \tag{17}$$

$$\frac{\partial F}{\partial \rho_g} = -\frac{(xS+1-x)x}{A_{x-s}S\rho_g^2} = \frac{\Phi_4}{A_{x-s}} \tag{18}$$

$$\frac{\partial F}{\partial A_{x-s}} = -\frac{1}{A_{x-s}}(xS+1-x)\frac{S(1-x)+x\frac{\rho_f}{\rho_g}}{S\rho_f} = \frac{\Phi_5}{A_{x-s}} \tag{19}$$

In Eq. (14), all variables, except $\partial S/\partial P$, $\partial S/\partial x$ and $\partial x/\partial z$, are known. Therefore, the choking relation can be obtained from the momentum equation if the constitutive relations for $\partial S/\partial P$, $\partial S/\partial x$ and $\partial x/\partial z$ are established. Indeed, these parameters are the keys in solving the critical flow of the two-phase flow because they reflect the degree of the mechanical and thermal non-equilibrium. While $\partial S/\partial P$ is related to the mechanical non-equilibrium and $\partial x/\partial z$ is related to the thermal non-equilibrium, respectively, $\partial S/\partial x$ is the parameter that account for both mechanical and the thermal non-equilibrium.

In the present analysis, the drift flux model is introduced to provide constitutive relations for $\partial S/\partial P$ and $\partial S/\partial x$ such that the slip ratio is written as

$$S = C_o + \frac{x(C_o - 1)\rho_f}{\rho_g(1-x)} + \frac{\rho_f \langle\langle V_{gj}\rangle\rangle}{G(1-x)} \tag{20}$$

The distribution parameter, C_o, indicates the effect of the radial void fraction and volumetric flux distribution. The drift velocity, $\langle\langle V_{gj}\rangle\rangle$ is a measure of the local slip. The distribution parameter and drift velocity are depending on the flow regime and flow component.

The remarkable difference between the two-phase one-component flow and two-phase two-component flow is that there is a phase change in the former. Therefore, the considerations for the phase change are required to analyze two-phase one-component flow. In Eq. (14), several terms are related to the quality change, namely, phase change.

The parameter $\partial x/\partial z$ is related to the phase change. Here, it is required to define the quality change to calculate $\partial x/\partial z$ analytically. In this research, the quality change is defined as

$$\Delta x = \Delta x_{eq}\left(1 - e^{-\frac{\tau_{char}}{\tau_{dep}}}\right) \tag{21}$$

where τ_{char} and τ_{dep} are the characteristic time and the bubble departure time for bubble growth to depart. Here, x_{eq} indicates the equilibrium quality that is defined as

$$x_e = (h_{in} - h_f)/h_{fg} \tag{22}$$

The term in the bracket of Eq. (21) is the degree of the thermal non-equilibrium based on the relaxation of the flashing. If τ_{dep} is zero, the quality is the same as the equilibrium quality. This is the case for thermal equilibrium. If the bubble departure time, τ_{dep}, is infinite, then the actual quality is zero. This means that there is no flashing. The characteristic time is the function of the geometry and flow. The characteristic time is defined as

$$\tau_{char} = L/V_f \tag{23}$$

where L is the length of test section. Therefore, as L gets longer, there is less thermal non-equilibrium in the fixed bubble departure time. This means that the nozzle geometry has more chance to be thermal equilibrium than the orifice. If the characteristic time is much longer than the bubble departure time ($\tau_{char} \gg \tau_{dep}$), it reaches the thermal equilibrium. The vise verse case means the complete thermal non-equilibrium. As mentioned before, τ_{dep} is the bubble departure time from the wall. The bubble which is generated at the wall requires some time to depart the wall. In this processing, the energy is transferred by the conduction between the superheated liquid and vapor. When the bubble size reaches to the bubble departure size, the bubble may depart. To estimate the bubble departure time, the frequency of bubble departures which was developed by Zuber [31] is adopted here, thus

$$D_d f_d = 1.18\left[\frac{\sigma g(\rho_f - \rho_g)}{\rho_f^2}\right]^{1/4} \tag{24}$$

where D_d and f_d denotes a bubble departure diameter and bubble generation frequency. In Eq. (24), the inverse of frequency represents the bubble departure time. The frequency of bubble departure is composed of delayed time, τ_d, and break-off time, τ_b, as

$$f_d = \frac{1}{\tau_{dep}} = \frac{1}{\tau_b + \tau_d} \tag{25}$$

After the departure of a bubble, liquid at the bulk fluid temperature comes in contact with the solid and gets heated. A brief period of time then elapsed, during which transient conduction into the liquid occurs but no bubble growth takes place. This time is the delayed time. This time depends on the condition vicinity of the nucleating cavity, i.e. on the local heating rate, thermal fluctuations in the liquid, and the radius of the cavity [31]. The break-off time means the bubble growth time until it departs from the wall. Actually, this break-off time is same with the conduction time which is explained. The duration of the break-off time depends on the local superheat temperature difference and on the local hydrodynamic condition. Actually the bubble departure is governed by the dynamics of the surrounding liquid as well as by the buoyant and adhesion force. The bubble departure diameter is determined by Kocamustafaogullari's model [32] given by

$$D_d = 2.64 \times 10^{-5}\theta\left(\frac{\sigma}{g\Delta\rho}\right)^{0.5}\left(\frac{\Delta\rho}{\rho_g}\right)^{0.9} \tag{26}$$

where θ and $\Delta\rho$ are contact angle and density difference between liquid and vapor, respectively. The contact angle is assumed as 38° which was calculated by Xu et al. [33]. Therefore, the bubble departure time is expressed as

$$\tau_{dep} = \frac{1}{f_d} = \frac{2.64 \times 10^{-5}\theta\left(\frac{\sigma}{g\Delta\rho}\right)^{0.5}\left(\frac{\Delta\rho}{\rho_g}\right)^{0.9}}{1.18\left[\frac{\sigma g\Delta\rho}{\rho_f^2}\right]^{1/4}} \tag{27}$$

The next procedure is to calculate the $\partial x/\partial z$ based on the defined quality.

$$\frac{dx}{dz} = \frac{d}{dz}\left(x_e\left(1 - e^{-\frac{\tau_{char}}{\tau_{dep}}}\right)\right) = \left(1 - e^{-\frac{\tau_{char}}{\tau_{dep}}}\right)\frac{dx_e}{dz} \tag{28}$$

In Eq. (28), dx/dz is expressed with dx_e/dz. Therefore, more detailed consideration is required in the analysis of dx_e/dz. In general, the flashing is related to the pressure and pressure drop. And the equilibrium quality follows the thermodynamic path line. Hence, dx_e/dz is given by

$$\frac{dx_e}{dz} = \frac{dx_e}{dP}\frac{dP}{dz} \tag{29}$$

From Eq. (22), $\partial x_e/\partial z$ is transformed as

$$\begin{aligned}\frac{dx_e}{dz} &= -\frac{d}{dP}\left(\frac{h_i - h_f}{h_{fg}}\right)\frac{dP}{dz} \\ &= \left(-\frac{1}{h_{fg}}\frac{dh_f}{dP} - \frac{h_i - h_f}{h_{fg}^2}\frac{dh_{fg}}{dP}\right)\frac{dP}{dz}\end{aligned} \tag{30}$$

From the definition of enthalpy, the enthalpy difference for each phase is described as

Liquid

$$dh_f = c_p\,dT + (1-\beta)\frac{dP}{\rho} \tag{31}$$

Vapor

$$dh_g = c_p\,dT \tag{32}$$

Here, β is the volumetric thermal expansion coefficient, and defined as

$$\beta \equiv -\frac{1}{\rho}\frac{\partial\rho}{\partial T}\bigg|_P \tag{33}$$

By inserting Eqs. (31) and (32) into Eq. (30), the quality change is given by

$$\begin{aligned}\frac{dx_e}{dz} = -\Bigg[&\frac{1}{h_{fg}}\left(c_{p_f}\frac{dT}{dP} + \frac{1-\beta T}{\rho_f}\right) + \frac{h_i - h_f}{h_{fg}^2} \\ &\times\left(c_{pg}\frac{dT}{dP} - c_{p_f}\frac{dT}{dP} - \frac{1-\beta T}{\rho_f}\right)\Bigg]\frac{dP}{dz}\end{aligned} \tag{34}$$

The Clapeyron equation explains the relationship between the pressure and the temperature on the saturation condition as following

$$\left(\frac{dP}{dT}\right)_{sat} = \frac{\rho_g h_{fg}}{T} \tag{35}$$

By using the Clapeyron equation, the final equation for the phase change is obtained as

$$\begin{aligned}\frac{dx_e}{dz} = -\Bigg[&\frac{1}{h_{fg}}\left(\frac{c_{p_f}T}{h_{fg}\rho_g} + \frac{1-\beta T}{\rho_f}\right) + \frac{h_i - h_f}{h_{fg}^2} \\ &\times\left(\frac{c_{p_g}T}{h_{fg}\rho_g} - \frac{c_{p_f}T}{h_{fg}\rho_g} - \frac{1-\beta T}{\rho_f}\right)\Bigg]\frac{dP}{dz}\end{aligned} \tag{36}$$

By inserting Eq. (36) into Eq. (28), the finalized $\partial x/\partial z$ is obtained.

$$\begin{aligned}\frac{dx}{dz} &= -\Bigg[\frac{1}{h_{fg}}\left(\frac{c_{p_f}T}{h_{fg}\rho_g} + \frac{1-\beta T}{\rho_f}\right) + \frac{h_i - h_f}{h_{fg}^2} \\ &\quad\times\left(\frac{c_{p_g}T}{h_{fg}\rho_g} - \frac{c_{p_f}T}{h_{fg}\rho_g} - \frac{1-\beta T}{\rho_f}\right)\Bigg]\left(1 - e^{-\frac{\tau_{char}}{\tau_{dep}}}\right)\frac{dP}{dz} \\ &= \xi_1\frac{dP}{dz}\end{aligned} \tag{37}$$

Eq. (37) shows that the dx/dz is related to the choking flow rate because it is coupled with the pressure drop. Based on Eqs. (37) and (14) needs to be modified by considering the phase change. For the first term in the parenthesis of Eq. (14), the derivative with respect to the quality needs to be considered. Therefore, this term needs to be modified for the two-phase one-component flow as

$$\begin{aligned}&\frac{\partial F}{\partial S}\frac{\partial S}{\partial P}\frac{\partial P}{\partial z} \\ &= \frac{\partial F}{\partial S}\left(\frac{\partial S}{\partial C_o}\frac{\partial C_o}{\partial P} + \frac{\partial S}{\partial x}\frac{\partial x}{\partial P} + \frac{\partial S}{\partial \rho_f}\frac{\partial \rho_f}{\partial P} + \frac{\partial S}{\partial \rho_g}\frac{\partial \rho_g}{\partial P}\right)\frac{\partial P}{\partial z} \\ &= \frac{\partial F}{\partial S}\left(\frac{\partial S}{\partial C_o}\frac{\partial C_o}{\partial P} + \frac{\partial S}{\partial \rho_f}\frac{\partial \rho_f}{\partial P} + \frac{\partial S}{\partial \rho_g}\frac{\partial \rho_g}{\partial P}\right)\frac{\partial P}{\partial z} + \frac{\partial F}{\partial S}\frac{\partial S}{\partial x}\frac{\partial x}{\partial z}\end{aligned} \tag{38}$$

As noticed in Eq. (38), the same term with the second term of parenthesis in Eq. (14) is generated. For this term $\partial S/\partial x$ is obtained from Eq. (20).

$$\frac{\partial S}{\partial x} = \frac{(C_o - 1)\rho_f}{\rho_g(1-x)^2} + \frac{\rho_f\langle\langle V_{gj}\rangle\rangle}{G(1-x)^2} = \Pi_1 \tag{39}$$

Therefore, by using Eqs. (15), (37) and (39) the second term in Eq. (38) is written as

$$\frac{\partial F}{\partial S}\frac{\partial S}{\partial x}\frac{\partial x}{\partial z} = \frac{\Phi_1\Pi_1}{A_{x-s}}\left(\xi_1\frac{dP}{\partial z}\right) \tag{40}$$

In two-phase one-component flow, the distribution parameter, C_o, is different from that of two-phase two-component flow. The developed correlation by Ishii [28] is given by

$$C_o = \left(1.2 - 0.2\sqrt{\frac{\rho_g}{\rho_f}}\right)\left(1 - e^{-18\alpha}\right) \quad \text{for } \alpha \leqslant 0.75 \tag{41}$$

$$C_o = 1 + (1-\alpha)\Bigg/\left\{\alpha + \left[\frac{1 + 75(1-\alpha)}{\sqrt{\alpha}}\frac{\rho_g}{\rho_f}\right]^{1/2}\right\} \quad \text{for } \alpha > 0.75 \tag{42}$$

Therefore, as an example, for $\alpha \leqslant 0.8$ $\partial C_o/\partial\rho_g$ and $\partial C_o/\partial\rho_f$ are obtained as follows

$$\frac{\partial C_o}{\partial \rho_g} = -0.1\left(\frac{1}{\rho_g\rho_f}\right)^{1/2}\left(1 - e^{-18\alpha}\right) = \Psi_1 \tag{43}$$

$$\frac{\partial C_o}{\partial \rho_f} = \frac{0.1}{\rho_f}\left(\frac{\rho_g}{\rho_f}\right)^{1/2}\left(1 - e^{-18\alpha}\right) = \Psi_2 \tag{44}$$

By inserting all adequate derivatives into Eq. (14), the momentum equation which considers the phase change is given by

$$-\frac{\mathrm{d}P}{\mathrm{d}z}=\frac{\dot{m}^2}{A_{x-s}}\left[\begin{array}{c}\dfrac{\Phi_1(\Omega_1\Psi_2+\Omega_2)}{A_{x-s}}\dfrac{\partial\rho_\mathrm{f}}{\partial P}\dfrac{\partial P}{\partial z}+\dfrac{\Phi_1(\Omega_1\Psi_1+\Omega_3)}{A_{x-s}}\dfrac{\partial\rho_\mathrm{g}}{\partial P}\dfrac{\partial P}{\partial z}+\dfrac{2\Phi_1\Pi_1}{A_{x-s}}\left(\xi_1\dfrac{\partial P}{\partial Z}\right)\\ +\dfrac{\Phi_2}{A_{x-s}}\left(\xi_1\dfrac{\partial P}{\partial Z}\right)+\dfrac{\Phi_3}{A_{x-s}}\dfrac{\partial\rho_\mathrm{f}}{\partial P}\dfrac{\partial P}{\partial z}+\dfrac{\Phi_4}{A_{x-s}}\dfrac{\partial\rho_\mathrm{g}}{\partial P}\dfrac{\partial P}{\partial z}+\dfrac{\Phi_5}{A_{x-s}}\dfrac{\partial A_{x-s}}{\partial z}\end{array}\right] \tag{45}$$

Based on the obtained parameters, the momentum equation is rearranged as

$$-\left[1+G^2\left(\begin{array}{c}\Phi_1(\Omega_1\Psi_2+\Omega_2)\dfrac{\partial\rho_\mathrm{f}}{\partial P}+\Phi_1(\Omega_1\Psi_1+\Omega_3)\dfrac{\partial\rho_\mathrm{g}}{\partial P}\\ +2\Phi_1\Pi_1\xi_1+\Phi_2\xi_1+\Phi_3\dfrac{\partial\rho_\mathrm{f}}{\partial P}+\Phi_4\dfrac{\partial\rho_\mathrm{g}}{\partial P}\end{array}\right)\right]\frac{\mathrm{d}P}{\mathrm{d}z}=G^2\left(\Phi_5\frac{\partial A_{x-s}}{\partial z}\right) \tag{46}$$

The choking condition occurs when the bracket on the left hand side in Eq. (46) equals zero, i.e.,

$$G^2=\frac{-1}{(\Phi_1\Omega_1\Psi_2+\Phi_1\Omega_2+\Phi_3)\dfrac{\partial\rho_\mathrm{f}}{\partial P}+(\Phi_1\Omega_1\Psi_1+\Phi_1\Omega_3+\Phi_4)\dfrac{\partial\rho_\mathrm{g}}{\partial P}+(2\Phi_1\Pi_1+\Phi_2)\xi_1} \tag{47}$$

According to Eq. (47), the choking flow rate is composed of gas sonic velocity, liquid sonic velocity and phase change factor. The mechanical non-equilibrium factor is coupled with the gas and liquid sonic velocity. However, the thermal non-equilibrium factor is just coupled with slip ratio itself.

In the two-phase one-component flow, one of the main characteristics is the flashing. In the test section, the pressure drop caused by the acceleration is the dominant factor to make the flashing (the frictional pressure drop in the choking flow is negligible compared to the accelerative pressure drop). The consideration for the thermal non-equilibrium is important in case of the flashing.

For the flow with subcooled inlet condition, there are two types of choking flow, one is subcooled water choking and the other is two-phase choking. For example, the water with small subcooled inlet condition in the nozzle, the pressure drop is caused by the acceleration and the pressure may reaches the saturation pressure corresponding to the inlet water temperature. If the exit pressure of the nozzle is less than the nucleation pressure (pressure undershoot for nucleation), the nozzle exit condition is two-phase flow even though there is thermal non-equilibrium. In this condition, the choking flow needs to be calculated based on the two-phase choking condition with the relaxation model as was described before. However, if the degree of subcooling is relatively high, then the exit pressure of the nozzle will be still higher than the saturation pressure corresponding to the inlet water temperature. The flashing also happens in this condition, however, the two-phase choking model cannot be used for the highly subcooled water flow. Therefore, the additional modeling is required to analyze the whole choking flow with subcooled inlet condition. Alamgir and Lienhard [34] developed the following correlation for the rapid depressurization of subcooled water on the basis of classical nucleation theory for pressure undershoot

$$\Delta P_\mathrm{fl}=P_{s,T_\mathrm{in}}-P_\mathrm{fl}=\left[0.258\sigma^{3/2}T_\mathrm{r}^{13.76}\left(1+13.25\Sigma^{0.8}\right)^{0.25}\right]\Big/\left[(k_\mathrm{s}T_\mathrm{c})^{0.5}\left(1-\frac{\rho_\mathrm{g}}{\rho_\mathrm{f}}\right)\right] \tag{48}$$

where ΔP_fl is the pressure undershoot relative to the saturation pressure at flashing, P_{s,T_i} the saturation pressure corresponding to the inlet water temperature, P_fl the flashing pressure, σ the surface tension, k_s Boltzmann's constant, T_c the critical temperature, Σ the rate of depressurization in Matm/s, T_r the reduced temperature, or the ratio of initial water temperature to critical temperature. To apply the correlation for the test of Reocreux [19] and Zimmer et al. [20], Levy and Abdollahian [18] modified the correlation:

$$\Delta P_\mathrm{fl}=\left[0.258\sigma^{3/2}T_\mathrm{r}^{13.76}\left(0.49+13.25\Sigma^{0.8}\right)^{0.25}\right]\Big/\left[(k_\mathrm{s}T_\mathrm{c})^{0.5}\left(1-\frac{\rho_\mathrm{g}}{\rho_\mathrm{f}}\right)\right] \tag{49}$$

Amos and Schrock [35] proposed the simple modification to Eq. (49), which attempts to extend the correlation to lower rates of depressurization. The proposed correlation with multiplier (varying from 0.1 to 0.9) considering the velocity is given by

$$\Delta P_{\mathrm{fl}} = J\left[\frac{0.258\sigma^{3/2}T_{\mathrm{r}}^{13.76}(0.49+13.25\Sigma^{0.8})^{0.25}}{(k_{\mathrm{s}}T_{\mathrm{c}})^{0.5}\left(1-\frac{\rho_{\mathrm{g}}}{\rho_{\mathrm{f}}}\right)}\right] \tag{50}$$

Based on Eq. (50), it is possible to estimate the pressure for flashing. In the TRACE code, the choking mass flux for highly subcooled water is calculated using the Bernoulli equation with the inlet pressure and nucleation pressure. The velocity based on the Bernoulli equation is given by

$$V_{\mathrm{Bernoulli}} = \left[V_{\mathrm{exit}}^2 + \frac{(P_{\mathrm{exit}} - P_{\mathrm{fl}})}{\rho_{\mathrm{exit}}}\right]^{1/2} \tag{51}$$

where P_{exit} is the pressure at the exit, P_{fl} flashing pressure, ρ_{exit} liquid density at the exit and V_{exit} exit liquid velocity. Therefore, the choking mass flux for highly subcooled water is given by

$$G_{\mathrm{c}} = V_{\mathrm{Bernoulli}} \cdot \rho_{\mathrm{exit}} \tag{52}$$

According to TRACE manual [36], it is suggested to use the multiplier for calculated choking velocity based on Eq. (50). In this research, it was found that Eq. (50) overpredicted the Purdue data whereas it underpredicted the test data as the degree of subcooling decreased. Hence, Eq. (52) is modified as

$$G_{\mathrm{c}} = 1.6094 V_{\mathrm{Bernoulli}} \cdot \rho_{\mathrm{exit}} \cdot (T_{\mathrm{sat,exit}} - T_{\mathrm{in}})^{-0.1918} \tag{53}$$

where $T_{\mathrm{sat,exit}}$ and T_{in} denote the saturation temperature corresponding to the exit pressure and the inlet or initial water temperature.

The choking mass flux is obtained by solving the momentum equation in the test geometry (nozzle). In the calculation of the pressure drop through the nozzle, the choking model was automatically chosen based on the calculated pressure and inlet temperature in each node. If the exit pressure is higher than the saturation pressure corresponding to the inlet temperature, the Bernoulli choking model is chosen to calculate the choking mass flux. The two-phase relaxation model is used when there exits two-phase flow at the upstream of the choking point due to the pressure drop.

In the previous section, the thermal non-equilibrium quality change was defined as Eq. (21). This thermal non-equilibrium quality change is defined based on the mechanistic model. Therefore, it is modified to fit the data by introducing the multiplier as

$$\Delta x = \Delta x_{\mathrm{eq}}\left(1 - \mathrm{e}^{-\frac{\tau_{\mathrm{char}}}{\tau_{\mathrm{dep}}}}\right)\left(-0.2783\frac{P_{\mathrm{o}}}{P_{\mathrm{c}}} + 0.2266\right) \tag{54}$$

where P_{o} is the inlet pressure and P_{c} critical pressure. $P_{\mathrm{o}}/P_{\mathrm{c}}$ means the reduced pressure. Currently Eq. (54) is verified up to the pressure of 8.54 MPa. Probable, it may be required to modify the multiplier to apply for higher pressure condition.

4. Results

The developed choking flow model, equation is compared with the experimental data for the nozzle geometry [37]. The choking flow experiments were performed using PUMA (Purdue University Multidimensional integral test Assembly) facility of PURDUE University. The PUMA test facility is a scaled integral model of the General Electric Nuclear Energy, simplified Boiling Water Reactor (SBWR) [38,39]. Experimental upstream pressure conditions were 0.207 MPa, 0.345 MPa, 0.517 MPa, 0.689 MPa, and 1.034 MPa.

The reactor pressure vessel (RPV) and drywell were used as the pressure boundary in this experiment. The RPV was used as the upstream stagnation reservoir and the drywell was used as the downstream receiver with the horizontal test section connected between the RPV and the drywell. The inner diameter of the test section was 25.4 mm except at the choking section. The throat size was 5.4 mm in both geometries.

Fig. 2 shows the model prediction which considered the single phase subcooled water and relaxation of flashing. The considered model predicts the experimental data quite well.

According to the comparison of the predicted choking mass flux with the experimental data (Fig. 3(a)–(e)), the model reasonably predicts the choking mass flux in the broad range of subcooling. As can be seen in the figures, there is a discontinuity region due to the different model used depending on the flow condition. In this unstable region, converged values are unreasonable or there is no convergence. However, this problem can be solved if the numerical calculation method is improved. At the boundary between two models, the Bernoulli model quite underpredicts the data because the degree of subcooling is decreased, therefore, the pressure difference between flashing pressure and exit pressure is reduced. Hence, the predicted velocity is decreased. In general, both models predict the experimental data well except for the boundary which was mentioned before. In Eq. (47), the choking mass flux is composed of the liquid sonic velocity, gas sonic velocity, and phase change related term. In the calculation of choking mass flux, the first and third term of the denominator in Eq. (47) are positive, which means that these terms are increasing the predicted choking mass flux. At the low void fraction, absolute value of the flashing related term is greater than that of the gas sonic velocity term, hence, the denominator becomes the positive. The Bernoulli choking model naturally prevents this problem.

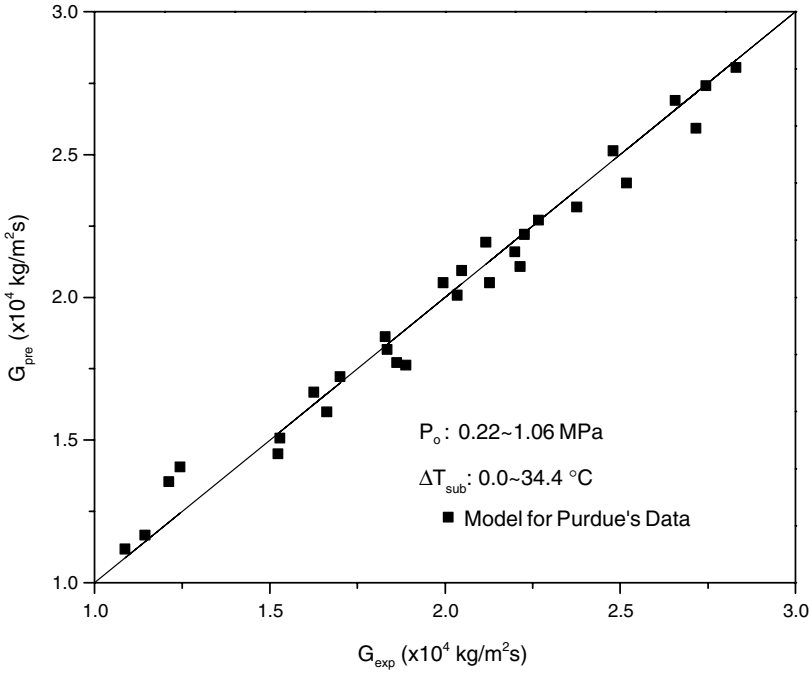

Fig. 2. Comparison of predicted choking mass flux with Purdue data.

The developed non-homogeneous non-equilibrium model is assessed by comparing with other experimental data. The developed model is compared with subcooled water and steam water experimental data.

As the comparable experiment for the subcooled water flow, Xu et al.'s [33] experimental data is chosen to assess the developed model in the high pressure. They performed the choking flow experiment with 3.0–16.0 MPa pressure and 1–60 °C inlet liquid stagnation subcooling. The test section geometry is the converging-diverging nozzle with 30 mm inlet diameter, 4.18 mm throat diameter, and 25.4 mm outlet diameter. The half angle of the convergent section is 30°.

Among the experimental data, the data below 8.54 MPa stagnation pressure are chosen to compare with the model prediction. According to Fig. 4, the model predicts the choking mass flux with the error range from −1.2% to 3.1%. This means the developed model is applicable in both high and low pressure conditions. According to the code calculation, a majority of choking calculation is done by the two-phase choking model because the exit pressure is lower than the pressure corresponding to the inlet temperature due to the acceleration in the nozzle for most cases.

One of the flow patterns of the two-phase one-component flow is the steam-water flow. Therefore, to ensure that the developed model would be applicable for this condition, it is imperative that the separate effect test with steam-water flow should be used as part of the model assessment. The chosen separate effect test for steam-water choking flow was that of Deich [40]. The nozzle geometry was a relatively smooth converging-diverging nozzle with 70 mm inlet diameter, 32.55 mm throat diameter, and 40 mm outlet diameter. The upstream pressure for the test was 0.122 MPa and the inlet quality varied from 0.15 to 0.998.

Based on the same model and solving methodology with the subcooled water flow, the choking mass flux is obtained for the steam-water flow. This result is shown in Fig. 5. The predicted choking mass flux is much higher than that of the experiment in the relatively low quality region. However, the void fraction in the low quality region is already higher than 0.95, which means that the flow regime is the annular flow. The slip ratio based on the original C_o is above than 20 and increases as the quality increases. Due to the large discrepancy, the sensitivity analysis is performed for the distribution parameter, C_o. For the sensitivity analysis, Eq. (42) is modified as

$$C_o = 1 + k\left(\frac{1-\alpha}{\alpha + \left[\frac{1+75(1-\alpha)}{\sqrt{\alpha}}\frac{\rho_g}{\rho_f}\right]^{1/2}}\right) \tag{55}$$

here, k is the control parameter for C_o. Three different values for k are tested ($k = 0.9$, 0.5, and 0.0). As C_o decreases by reducing k value, it is noticed that the discrepancy at the relatively low quality region gets smaller

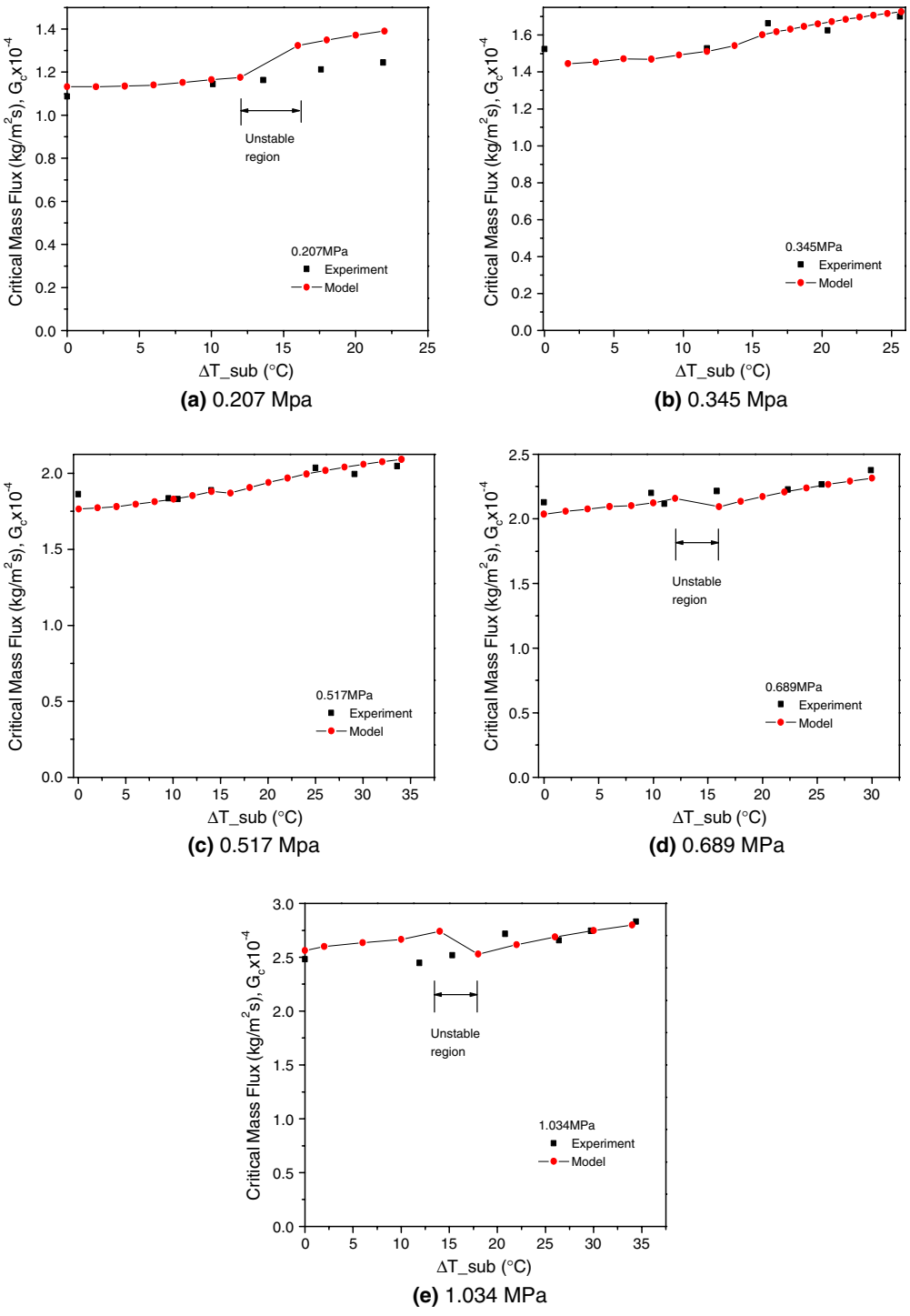

Fig. 3. Comparison of predicted choking mass flux with Purdue data for several pressures.

(Fig. 5). This is caused by the reduced slip ratio. Actually, the slip ratio with unity of C_o, which indicates that the flow is the homogeneous flow.

According to the results, the homogeneous flow predicts the experimental data quite well. However, in general, it is thought that the slip ratio in the annular flow

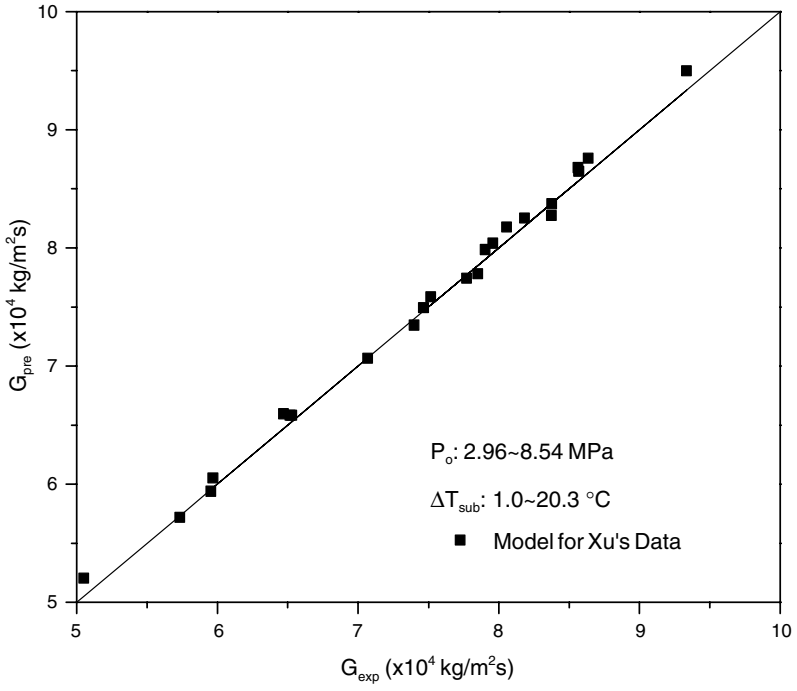

Fig. 4. Comparison of predicted choking mass flux with Xu data.

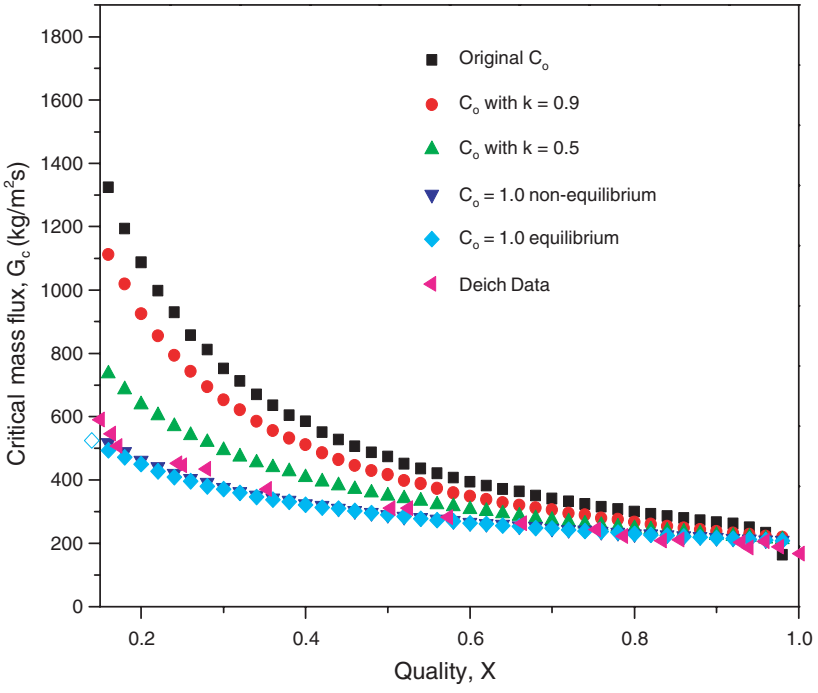

Fig. 5. Sensitivity analysis for C_o.

regime is large. Hence, it can be explained in view of the flow regime. In the very high void fraction region, flow regime may be the inverted annular flow. In the very high void fraction region, the liquid film thickness is

very thin, and the liquid can be entrained into the gas core when the bubble which is generated at the wall is detached from the wall. In this flow regime, the slip ratio may be near the unit. Hence, the model prediction with unit slip ratio shows the good agreement with the experimental data.

Based on this analysis, Eq. (55) is modified to reflect the flow regime change as

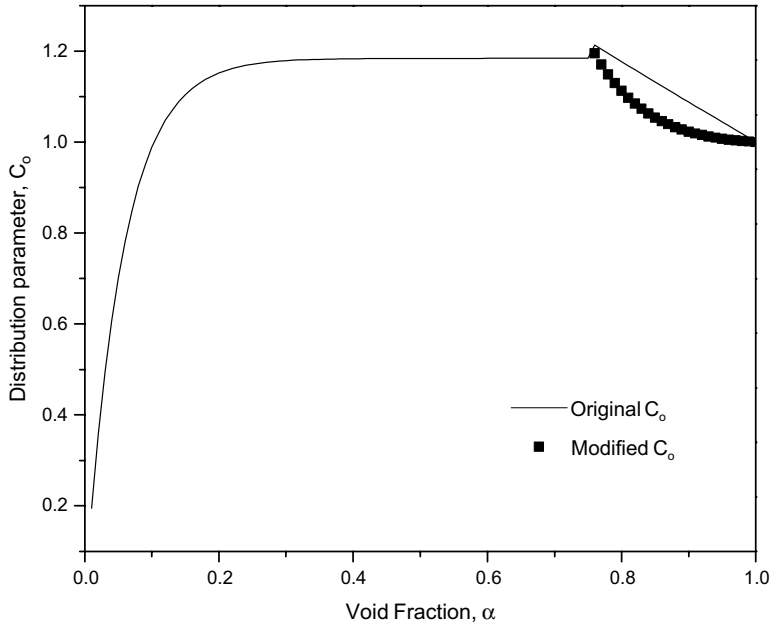

Fig. 6. Distribution parameter, C_o.

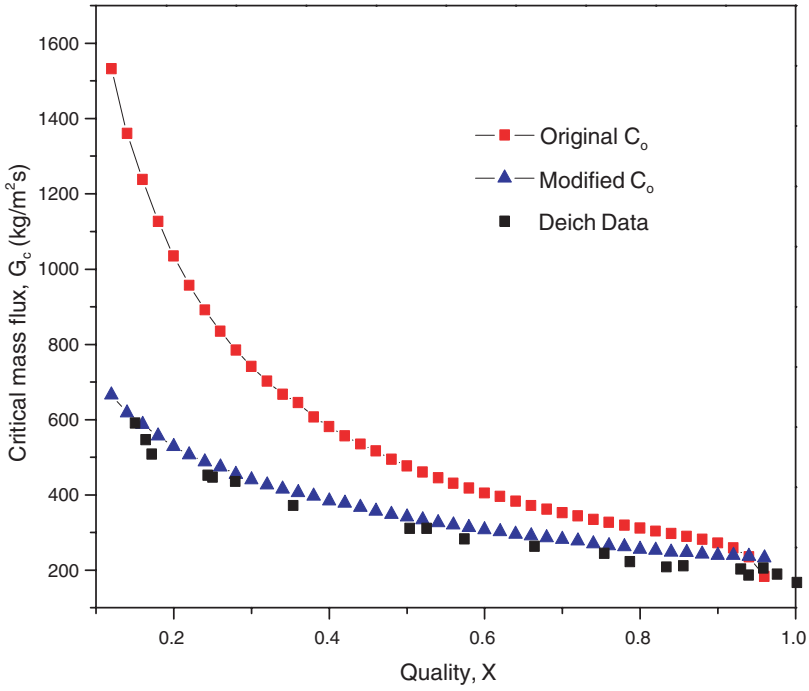

Fig. 7. Comparison of predicted choking mass flux with Deich data.

$$C_o = 1 + \left(\frac{1-\alpha}{\alpha + \left[\frac{1+75(1-\alpha)}{\sqrt{\alpha}} \frac{\rho_g}{\rho_f} \right]^{1/2}} \right) \exp[-9.0(\alpha - 0.75)] \quad (56)$$

In general, the flow is classified as the annular flow when the void fraction is higher than 0.75. Therefore, the multiplier in Eq. (56) accelerates the decreasing rate of C_o as the void fraction increases to consider the inverted annular flow. Fig. 6 shows the distribution parameter, C_o, for whole void fraction based on the used correlation depending on the flow regime. By modifying C_o for the annular flow regime based on Eq. (56), the decreasing rate of C_o is accelerated. Fig. 7 shows the model prediction with Deich's data after implementing Eq. (56).

5. Conclusions

The mechanistic model which considers the mechanical and thermal non-equilibrium for the two-phase choking flow is developed. In this research, the slip ratio which was defined in the drift flux model was used to identify the impact parameters on the slip ratio. Because the slip ratio in the drift flux model is related to the distribution parameter and drift velocity, the adequate correlations depending on the flow regime are introduced in this study. In this mechanistic modeling approach, the choking mass flow rate is expressed by the function of pressure, quality and slip ratio. For the thermal non-equilibrium, the relaxation model is introduced. This relaxation is composed of the characteristic time which is determined by the geometry and the flow condition and the bubble departure time. In this research, it is assumed that thermal equilibrium is established when a bubble depart from the wall. Hence, the amount of relaxation is controlled by the ratio of the characteristic time to bubble departure time.

For the two-phase one component flow, the mechanical and thermal non-equilibrium model (MTNEM) was developed with bubble conduction time and Bernoulli choking model. In case of highly subcooled water compared to the inlet pressure, the Bernoulli choking model using the pressure undershoot is used because there is not bubble generation in the test section. When the phase change happens inside the test section, two-phase choking model with relaxation time calculates the choking mass flux. According to the comparison of model prediction with experimental data shows good agreement. The developed model shows good prediction in both low and pressure ranges.

For the steam-water flow, the error between the model prediction and the experimental data is caused by the flow regime. In the high void fraction region, the flow regime may be the inverted annular flow. The slip ratio in the inverted flow regime is almost unit due to the thin liquid film, entrained liquid drop and bubble generation inside the liquid film. Therefore, the model prediction by modifying the distribution parameter, C_o, is accurate in this flow regime.

References

[1] V.E. Schrock, C.A. Amos, Two-phase Flow and Heat Transfer, China–US Seminar on Two-Phase Flows and Heat Transfer, Sian, China, 1984, pp. 115–138.

[2] Sauvage, Ecoulement de L'eau des Chaudieres, Annal. Mines 9, vol. II (1892).

[3] A. Rateau, Experimental Researches on the Flow of Steam through Nozzles and Orifice, to which is added a Note on the Flow of Hot Water, A. Constable and Co., Ltd, London, 1905.

[4] E.S. Starkman, V.E. Schrock, K.F. Neusen, D.J. Maneely, Expansion of a very low quality two-phase fluid through a convergent–divergent nozzle, J. Basic Engng, Trans. ASME, Ser. D 86 (2) (1964) 247–256;
W. Wulff et al., Quantifying Reactor Safety Margins, Part 3: Assessment and Ranging of Parameters, Nucl. Engng. Des. 119 (1990) 33–65.

[5] G.B. Wallis, Critical two-phase flow, Int. J. Multiphase Flow 6 (1980) 97–112.

[6] D. Abdollahian, J. Healzer, E. Janssen, C. Amos, Critical Flow Data Review and Analysis, Final Report, S. Levy, Inc. EPRI Report NP-2192, 1982.

[7] V.M. Fthenakis, U.S. Rohatgi, B.D. Chung, A simple model for predicting the release of a liquid-vapor mixture from a large break in a pressurized container, J Loss Prevent. Process Ind. 16 (2003) 61–72.

[8] R. Darby, Perspectives on Relief Valves Sizing for Two-phase Flow, International Symposium on Runaway Reactions, Pressure Relief Design, and Effluent Handling, Mach 11–13, New Orleans, Louisiana, 1998, pp. 365–397.

[9] M. Epstein, R.E. Henry, W. Midvidy, R. Pauls, One-dimensional Modeling of Two-phase Jet Expansion and Impingement, Thermal-Hydraulics of Nuclear Reactors II, 2nd Int. Topical Meeting on Nuclear Reactor Thermal-Hydraulics, Santa Barbara, CA, 1983.

[10] J.C. Leung, A generalized correlation for one-component homogeneous equilibrium flashing choked flow, AIChE J. 32 (1986) 1743–1746.

[11] J.C. Leung, M. Epstein, A generalized correlation for two-phase nonflashing homogeneous choked flow, J. Heat Transfer 112 (1990) 528–530.

[12] P. Saha, A Review of Two-Phase Steam-Water Critical Flow Models with Emphasis on Thermal Non-equilibrium, BNL-NUREG-50907, 1978.

[13] A group of expert of the NEA Committee on the Safety of Nuclear Installations, Critical Flow Modeling in Nuclear Safety, Nuclear Energy Agency, June 1982.

[14] S. Khajehnajafi, A. Shinde, Prediction of discharge rate from pressurized vessel blowdown through sheared pipe, Process Safety Progr. 14 (1) (1995) 22–25.

[15] V.E. Schrock, E.S. Starkman, R.A. Brown, Flashing flow of initially subcooled water in convergent–divergent nozzle, Trans. ASME, J. Heat Transfer 99 (1977) 263–268.
[16] H.K. Fauske, Flashing flows or: some practical guideline for emergency releases, Plant/Operat. Progr. 4 (3) (1985) 132–134.
[17] R.E. Henry, H.K. Fauske, The two-phase critical flow of one composition mixtures in nozzle, orifices, and short tubes, J. Heat Transfer 93 (1971) 179–187.
[18] S. Levy, D. Abdollahian, Homogeneous non-equilibrium critical flow model, Int. J. Heat Mass Transfer 25 (6) (1982) 759–770.
[19] M. Reocreux, Contribution à létude des debits critiques en enoulement diphasique eau-vapeur, Ph.D. thesis, Lúniversité Scientifique et médicale de Grenoble, 1974.
[20] G.A. Zimmer, B.J.C. Wu, W.J. Leonhardt, N. Abuaf, O.C. Jones, Pressure and Void Distributions in a Conversing-Diverging Nozzle with Non-equilibrium Water Vapor Generation, BNL-NUREG-26003, 1979.
[21] T. Lenzing, L. Friedel, J. Cremers, M. Alhusein, Prediction of the maximum full lift safety valve two-phase flow capacity, J. Loss Prevent. Process Ind. 11 (1998) 307–321.
[22] F.J. Moody, Maximum flow rate of a single component, two-phase mixture, Trans. ASME, J. Heat Transfer 86 (1965) 134–142.
[23] H.K. Fauske, Two-Phase Critical Flow with Application to Liquid Metal System, ANL-6633, 1963.
[24] H.K. Fauske, Contribution to the theory of two-phase, one-component critical flow, Ph.D. Thesis, 1962.
[25] P.A. Lottes, M. Petrick, J.F. Marchaterre, Lecture Notes on Heat Extraction from Boiling Water Power Reactors, Presented at the Advanced Summer Institute at Kjeller, Norway, August 17–29, ANL-6063, 1959.
[26] J.E. Cruver, R.W. Moulton, Critical flow of liquid vapor mixture, AIChE J. 13 (1) (1967) 52–60.
[27] J.A. Bouré, Two-Phase Flows with Application to Nuclear Reactor Design Problem, von Karman Institute for Fluid Dynamics, Lecture Series, Grenoble, France, 1974.
[28] M. Ishii, One-dimensional drift-flux model and constitutive equations for relative motion between phases in various two-phase flow regimes, ANL-77-47, 1977.
[29] J.A. Trapp, V.H. Ransom, A choked-flow calculation criterion for nonhomogeneous, nonequilibrium, two-phase flows, Int. J. Multiphase Flow 8 (6) (1982) 669–681.
[30] H.J. Richter, Separated two-phase flow model: application to critical two-phase flow, Int. J. Multiphase Flow 9 (5) (1983) 511–530.
[31] N. Zuber, Nucleate boiling. The region of isolated bubbles and the similarity with natural convection, Int. J. Heat Mass Transfer 6 (1963) 53–78.
[32] G. Kocamustafaogullari, Pressure dependence of bubble departure diameter for water, Int. Commun. Heat Mass Transfer 10 (6) (1983) 501–509.
[33] J.L. Xu, T.K. Chen, X.J. Chen, Critical flow in convergent–divergent nozzles with cavity nucleation model, Exp. Therm. Fluid Sci. 14 (1997) 166–173.
[34] M. Alamgir, J.H. Lienhard, Correlation of pressure undershoot during hot-water depressurization, J. Heat Transfer 103 (1981) 52–55.
[35] C.N. Amos, V.E. Schrock, Two-phase critical flow in slits, Nucl. Sci. Engng. 88 (1984) 261–274.
[36] J.W. Spore, J.S. Elson, S.J. Jolly-Woodruff, T.D. Knight, J.C. Lin, R.G. Nelson, C. Unal, J.H. Mahaffy, C. Murray, TRAC-M/FORTRAN 90 (Version 3.0) Theory Manual, LA-UR-00-910, 2000.
[37] H.J. Yoon, M. Ishii, S.T. Revankar, W. Wang, Simulation and Experimental Investigation of Mechanical and Thermal Non-equilibrium Effect on Choking Flow at Low Pressure, NUTHOS6, October 4–8, 2004, Nara, Japan, 2004.
[38] GE nuclear Energy, SBWR Standard Safety Analysis Report, Report No. 25A5113 Rev. A, 1992.
[39] M. Ishii, S.T. Revankar, T. Leonardi, R. Dowlati, M.L. Bertodano, I. Babelli, W. Wang, H. Pokharna, V.H. Ransom, R. Viskanta, J.T. Han, Scientific Design of Purdue University Multi-Dimensional Integral Test Assembly (PUMA) for GE SBWR, Purdue University Report PU-NE-94/1, US Nuclear Regulatory Commission Report NUREG/CR-6309, 1996.
[40] M.E. Deich, V.S. Danilin, G.V. Tsiklauri, V.K. Shanin, Investigation of the flow of wet steam in axisymmetric laval nozzles over a wide range of moisture content, High Temp. 7 (1969) 294–299.